

Local–Global Conformational Coupling in a Heptahelical Membrane Protein: Transport Mechanism from Crystal Structures of the Nine States in the Bacteriorhodopsin Photocycle

Janos K. Lanyi* and Brigitte Schobert

Department of Physiology and Biophysics, University of California, Irvine, California 92697

Received October 13, 2003; Revised Manuscript Received November 5, 2003

ABSTRACT: Proton pumps utilize a chemical or photochemical reaction to create pH and electrical gradients between the interior and the exterior of cells and organelles that energize ATP synthesis and the accumulation and extrusion of solutes and ions. G-protein coupled receptors bind agonists and assume signaling states that communicate with the coupled transducers. How these two kinds of proteins convert chemical potential to a proton transmembrane electrochemical potential or a signal are the great questions in structural membrane biology, and they may have a common answer. Bacteriorhodopsin, a particularly simple integral membrane protein, functions as a proton pump but has a heptahelical structure like membrane receptors. Crystallographic structures are now available for all of the intermediates of the bacteriorhodopsin transport cycle, and they describe the proton translocation mechanism, step by step and in atomic detail. The results show how local conformational changes propagate upon the gradual relaxation of the initially twisted photoisomerized retinal toward the two membrane surfaces. Such local–global conformational coupling between the ligand-binding site and the distant regions of the protein may be the shared mechanism of ion pumps and G-protein related receptors.

Bacteriorhodopsin (1–3) is a representative of a family of prokaryotic seven-transmembrane helical retinal proteins now known to be widespread in biology (4). In this light-driven pump, thermal reisomerization of the photoisomerized 13-cis,15-anti retinal back to all-trans (the photocycle) moves a proton from the cytoplasmic to the extracellular direction. Three decades of time-resolved and photostationary spectroscopy have defined the intermediate states of the photocycle in great detail, and by describing the path of the proton, established the outlines of transport mechanism. More recently, from spectroscopic changes in the visible and the infrared after flash photoexcitation and pH shifts, the local access hypothesis (5) identified the transport as the creation of transient bidirectional access for the Schiff base proton and the modulation of proton conductivities to and from this site that determine the cytoplasmic-to-extracellular directionality of the translocation.

Bacteriorhodopsin forms two-dimensional crystals in vivo (the purple membrane), well-suited for cryo-electron microscopy (6). With the cubic lipid phase method (7), it is possible to grow three-dimensional crystals that diffract to better than 2 Å (8, 9), and as far as 1.43 Å (10). Uniquely among ion pumps to date, crystallographic structures have been determined for all of the transport cycle intermediates (10–19), directly or indirectly and at various resolutions.

The nine crystallographic models provide the structural basis for the principle of the local access scheme (5), and this review combines what has been learned into a detailed and self-consistent atomic-level transport mechanism. It should be noted that the bacteriorhodopsin field is not without controversy. For example, an entirely different transport mechanism, based on other crystallographic measurements, was told elsewhere (20).

The central question of bacteriorhodopsin (i.e., how the excess free energy at the photoisomerized retinal is transferred to the rest of the protein to cause the motions required for proton translocation) is the same question posed for other ion pumps based on other driving reactions. It is similar to the question of how G-protein coupled membrane receptors function, where large-scale conformational changes are initiated by binding of the signaling molecule not with the rationale to mobilize the transported ion but to generate a conformation recognized as the signaling state by the coupled transducer.

Strategies for Determining the Structures of Photocycle Intermediates. The kinetic model of the proton transporting reaction sequence is approximated by the scheme, $BR-h\nu \rightarrow K \leftrightarrow L \leftrightarrow M_1 \leftrightarrow M_2 \rightarrow M_2' \leftrightarrow N \leftrightarrow N' \leftrightarrow O \rightarrow BR$, in which the spectral properties of the lettered states are well-described, and their molecular properties fulfill the need for distinct stages in the translocation of a proton (2). $L \leftrightarrow M_1$ corresponds to deprotonation of the retinal Schiff base, $M_1 \leftrightarrow M_2$ is the extracellular-to-cytoplasmic protonation switch,

* To whom correspondence should be addressed. Phone: (949) 824-7150. Fax: (949) 824-8540. E-mail: jlanyi@orion.oac.uci.edu.

Table 1: Structural Models^a Relevant to the Transport Mechanism Discussed

species	conditions of trapping	occupancy %	resolution, Å	PDB file	ref
BR (wild-type)	no illumination	100	1.47	1M0L	10
BR (wild-type)	no illumination	100	1.55	1C3W	9
K (wild-type)	green light, 100 K	40	1.43	1M0K	10
L (wild-type)	red light, 170 K	~60	1.62	1O0A	12
M ₁ (wild-type)	red light, 210 K	60	1.43	1M0M	13
M ₁ (wild-type)	yellow light, 230 K	100	2.00	1KG8	14
M ₁ (wild-type)	red light, 295 K	42	1.52	1P8H	18
M ₂ (in E204Q)	red light, 295 K	>93	1.80	1F4Z	15
M ₂ ' (in D96N)	red light, 295 K	100	2.00	1C8S	16
late M and N (in D96G/F171C/F219L)	no illumination (cryo-electron microscopy)	100	3.20	1FBK	17
N' (in V49A)	red light, 295 K	37	1.62	1P8U	18
O (D85S, no chloride)	no illumination	100	2.25	1JV7	19

^a From X-ray diffraction except where otherwise indicated.

M₂ → M₂' is the step where a proton is released to the extracellular surface (unidirectional at neutral pH), M₂' ↔ N corresponds to reprotonation of the Schiff base, N ↔ N' is where a proton is taken up from the cytoplasmic surface, N' ↔ O is the thermal reversion of the Schiff base, and O → BR is the final step where the Schiff base region regains its original charge state. Seven of these states have been trapped by rapidly cooling photostationary states (10–16, 18) in three-dimensional crystals of the wild-type protein or mutants to 100 K, where the diffraction data are collected. The conditions for the illumination were chosen to produce only one intermediate state, but in most cases, the photostationary mixtures contain unconverted protein also. Extracting the desired structures from such data is risky and requires the highest possible diffraction quality, convincing statistics from duplicate experiments, and adequate controls. The other two states of the cycle, N and O, exhibit large conformational changes and cannot be accumulated in three-dimensional crystals. Their structures are argued from crystallographic models of carefully chosen nonilluminated mutants (17–18). Of the 41 depositions from X-ray or electron diffraction of bacteriorhodopsin in the Protein Data Bank, Table 1 lists the 12 most relevant coordinate files.

The equivalence of the trapped states to those that arise transiently at ambient temperature may be judged from their FTIR and Raman spectra. The correspondence is good, but in K and L, some details are not entirely the same as in their higher temperature counterparts. This is an unavoidable problem of cryotrapping.

Retinal Dynamics During the Photocycle. The retinal in bacteriorhodopsin is near the center of the protein, surrounded by the seven helices, A through G, that traverse the membrane at nearly right angles to the surface (6). Its location defines an extracellular and a cytoplasmic half-channel that connects the retinal to the two membrane surfaces. In light-adapted bacteriorhodopsin, the retinal is all-trans, and the N–H of the protonated Schiff base formed with NZ of Lys-216 donates a hydrogen bond to wat402, which in turn donates hydrogen bonds to the anionic Asp-85 and Asp-212, residues on the extracellular side (8, 9). This arrangement is upset upon the absorption of a photon. Hydrogen-out-of-plane vibration of C₁₅–H and a lack of coupling between the C₁₄–C₁₅ stretch and the Schiff base in D₂O had indicated that in the K state, the retinal is a twisted 13-cis,15-anti (21, 22). As shown in Figure 1b, the distortion consists of partial

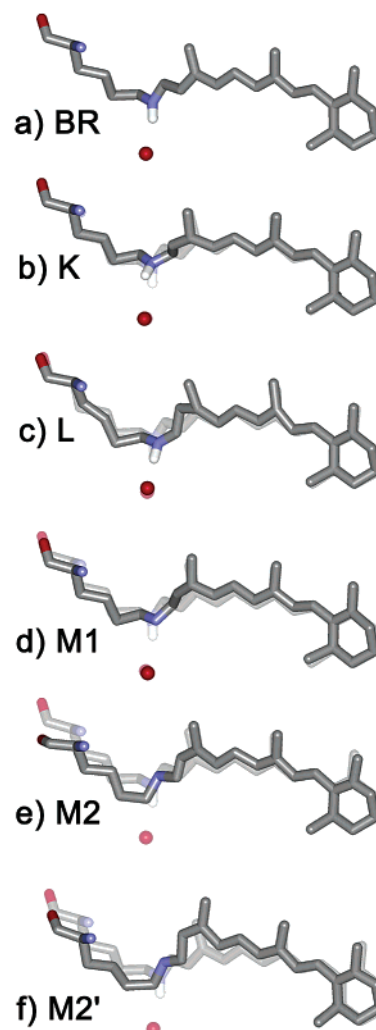


FIGURE 1: Motions of the retinal and wat402 in the first half of the photocycle. Panels a–f refer to the following states (with the PDB coordinate files in parentheses, cf. Table 1): a, BR (1M0L); b, K (1M0K); c, L (1O0A); d, M₁ (1M0M); e, M₂ (1F4Z); and f, M₂' (1C8S). A low-opacity image of panel a is included in panels b–f to illustrate the changes. Reproduced with permission from ref 12. 2003 Academic Press London.

counter-rotations of the C₁₄–C₁₅ and C₁₅=N bonds (10) that retain the extracellular direction of the N–H, but its hydrogen bond to wat402 is broken because the N–H–O angle becomes an unfavorable 116 ± 15°. Although at lower

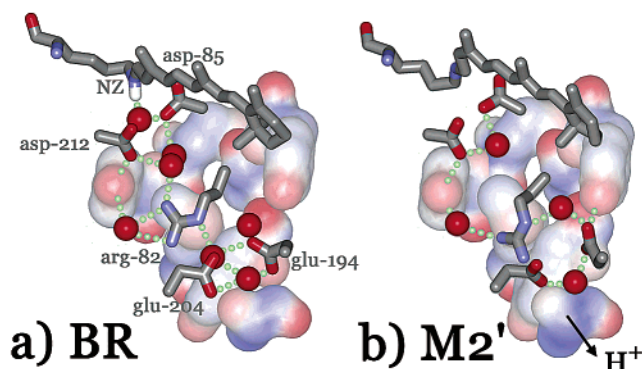


FIGURE 2: Structural changes in the extracellular region (including the retinal) between the BR (a) and the M_2' (b) states. Coordinate files 1MOL (a) and 1C8S (b). Color coded according to polarity, with red negative and blue positive. The extracellular surface, where a proton is released, is at the bottom of the figure.

resolution, this twisted retinal configuration is confirmed by the X-ray diffraction structure of K in another bacteriorhodopsin crystal with a different space group (11). Another distortion in these models is that the retinal remains linearly extended despite the rotated $C_{13}=C_{14}$ bond. The end-to-end distance of the retinal remains unchanged because the bond angle at C_{13} increases from 112 to $145 \pm 12^\circ$. The increased bond angle contains a large portion of the excess free energy in K. Clearly, this strained configuration (Figure 1b) is imposed on the isomerized retinal because in K the low compliance of the retinal binding site constrains the polyene chain.

In the subsequent steps of the photocycle, the C_{13} bond angle, and the retinal in general, gradually relax to a configuration similar to what it would assume in solution (i.e., with the polyene chain bent at C_{13} and the Schiff base rotated ca. 180° to face the other side (Figure 1)). Reaching this low-energy undistorted configuration requires that the Schiff base–Asp-85 interaction be broken (23). First, the Schiff base N–H bond is realigned with wat402 in the L intermediate (Figure 1c), consistent with FTIR evidence for reestablishment of its hydrogen bonding (22). Then, the proton of the Schiff base is lost to Asp-85 in the M_1 intermediate (Figure 1d), and finally the $C_{15}=NZ$ –CE segment (that includes the distal C atom of Lys-216) is rotated fully to the cytoplasmic side in the M_2 state (Figure 1e). With this rotation, and further relaxation of the C_{13} bond angle in M_2' (Figure 1f), the 13-cis retinal assumes its familiar bent shape. Wat402 leaves this region (or becomes disordered), and the connection of the deprotonated Schiff base with the extracellular region is broken. Reprotonation from the cytoplasmic side is thereby made possible, confirming the suggestion that the reversible kinetic step $M_1 \leftrightarrow M_2$ (5, 28) is the protonation switch in the pump.

Conformational Changes in the Extracellular Region: Proton Release. The Schiff base is connected to the extracellular surface by a continuous network of polar side chains and bound water. Little change in this region is evident at the current resolution of the crystallographic data until the Schiff base is deprotonated and the retylidene nitrogen rotates to the cytoplasmic side in M_2' . In this state, the network is collapsed (Figure 2b) because wat402 and wat406 disappear from the electron density map. Protonation of Asp-85 and the loss of the connection of the Schiff base/Asp-85 region

with Arg-82 allows its positively charged side chain to shift 1.7 \AA toward the Glu-194/Glu-204 pair near the extracellular surface (16). Approach of the positive charge causes the release of what appears to be a strongly delocalized proton (24), shared probably (25) between two water molecules as $H_5O_2^+$, to the bulk.

The release of the proton is coupled to rise of the pK_a of Asp-85 (26, 27). As the Arg-82 side chain flips toward the extracellular surface (Figure 2), the protonation equilibrium between Asp-85 and Schiff base is shifted toward more complete deprotonation. When the proton release is at a pH greater than the pK_a of the release site, the Arg-82 side chain will be arrested in its down position, the pK_a of Asp-85 remains high, and reprotonation of the Schiff base from the extracellular side is prevented. Through this coupling, the free energy dissipation in the release step adds unidirectionality to the otherwise bidirectional protonation switch (28).

At the end of the photocycle, Asp-85 reprotonates the vacant proton release site, possibly via Asp-212 (29). The outward tilt of the extracellular ends of helices A, D, and E in the O state (19) is accompanied by a rearrangement of side chains and water in the Arg-82/Glu-194/Glu-204 region, in preparation for this final proton transfer. It is only after deprotonation of Asp-85 as the BR state recovers that the side chain of Arg-82 returns to its initial position.

Conformational Changes in the Cytoplasmic Region: Reprotonation of the Schiff Base and Proton Uptake. In the late M state, the unprotonated Schiff base nitrogen points to the cytoplasmic direction, but its reprotonation from there requires that the high pK_a of the proton donor Asp-96 be lowered and that a proton-transfer pathway be built between donor and acceptor.

Thus, in the second half of the photocycle, the conformational changes are mainly in the cytoplasmic region. As the bent shape of the relaxed 13-cis,15-anti retinal is reached, the retinal binding pocket becomes distorted. The 13-methyl group is thrust against the indole ring of Trp-182, which tilts upward. The β -ionone ring of the retinal is fixed, but at the proximal end, the connected side chain of Lys-216 becomes more and more twisted, and in M_2 already (15), partially reverses the kink of helix G from the local π -helical turn (π -bulge) at Ala-215 and Lys-216. These displacements break the hydrogen bond between Trp-182 and wat501, disconnect helix F from Gly-215 on helix G, and cause repacking of the side chains between these helices. Beginning with M_1 , the repacking of side chains between helices F and G causes conformational changes that are communicated to Asp-96 where a cluster of water molecules is formed (13, 15, 18). In M_2 , Asp-96 and its hydrogen-bond partner, Thr-46, move part, and wat504 from the cluster intercalates between them. This cluster grows as larger conformational changes allow the influx of more water molecules.

Cryo-electron microscopy of two-dimensional crystals (30) produced projection structures for late M and N that indicated a distinct outward tilt of the cytoplasmic end of helix F and a less defined change of helix G. The motion of helix F and an inward tilt of helix G was confirmed by an X-ray projection map that revealed displacement of a Hg label at an engineered cysteine (31), spin–spin distance changes at the cytoplasmic surface (32, 33), and the accessibilities of engineered cysteines along the E–F interhelical loop (34). An image of the main-chain displacements is available from

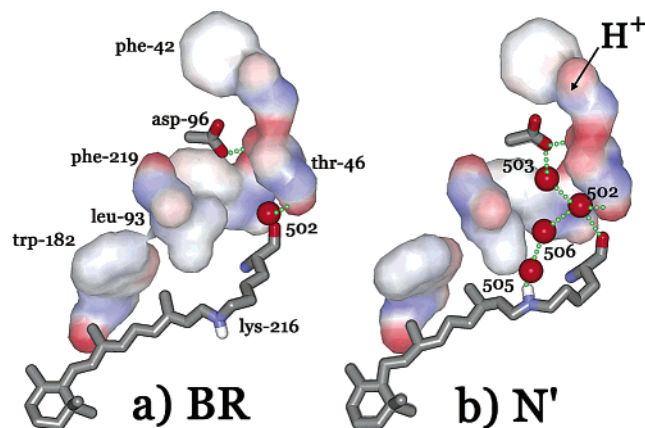


FIGURE 3: Structural changes in the cytoplasmic region (including the retinal) between the BR (a) and the N' (b) states. Coordinate files 1M0L (a) and 1P8U (b). Color coded according to polarity, with red negative and blue positive. The cytoplasmic surface, from where a proton is taken up, is at the top of the figure. Reproduced with permission from ref 3. 2003 Annual Review of Physiology.

the structure of a long-living N state in the F219L mutant from cryo-electron microscopy (35). As judged from projection structures, there are at least two mutants in which this open structure is assumed without illumination (17, 36). From one of these (17), some details of the conformational change were determined by cryo-electron microscopy, and its rationale was identified as the creation of a channel for proton conduction from the cytoplasmic surface to the Schiff base. No such changes have been seen in three-dimensional crystals; however, although in the M state produced in the D96N mutant (a late M), the cytoplasmic ends of helices F and G are disordered (16), suggesting that a tendency for a conformational change is opposed by the crystal lattice. This may be the reason that attempts to accumulate N and O in three-dimensional crystals have been unsuccessful.

By the time the N' state is formed, a continuous single-file of four hydrogen-bonded water molecules (18) connects the reprotonated Schiff base with the reprotonated Asp-96 (Figure 3b). One of these, wat502, was in the BR structure already, although displaced, while the other water molecules will have entered this region by filling cavities that form upon the repacking of side chains. Important for proton conduction (37), the string of water is located in a hydrophobic groove, and most of its hydrogen bonds are between neighboring water molecules and where it connects to the proton donor and acceptor. A propensity for accumulating water in this region is indicated by the fact that a cavity created by mutation of Phe-219 to Leu recruits two hydrogen-bonded waters to the existing wat501 (18).

Lowering the pK_a of Asp-96 and conduction of a proton from Asp-96 to the unprotonated Schiff base both involve entry of water into the protein, but they occur in distinct photocycle steps and are influenced by different conditions. On one hand, a cooperativity that seems to arise from lateral pressure in the lattice of the purple membrane from the conformational change of helix F affects specifically the pK_a of Asp-96 (38). On the other, proton exchange between Asp-96 and the Schiff base is specifically inhibited by osmotic and hydrostatic pressure, but without affecting the pK_a of Asp-96 (39, 40). The gradual accumulation of water clusters, first near Asp-96 and then between Asp-96 and the Schiff base, gives a structural rationale for these observations.

In contrast to these semistable clusters in the protein interior, after reprotonation of Asp-96, in N' and O, only what appears to be the disrupted remains of an aqueous chain can be observed (18) between Asp-96 and the cytoplasmic surface. Presumably, such a chain exists while Asp-96 becomes protonated, but transiently.

Coupling the Retinal Motions to Proton Translocation. The photocycle reactions are driven by excess free energy at the distorted retinal in the K state. In the first half of the cycle, the distortions of the retinal gradually disappear but at the expense of increasing conformational changes of the protein. Displacements of wat402 and side chains facilitate proton transfer between the Schiff base and Asp-85, and the resulting loss of their interaction allows rotation of the $C_{15}=N-CE$ segment. Displacements of Val-93, Leu-181, and Trp-182 remove steric conflict with the increasingly bent contour of the 13-cis retinal, and by the M_2' state, the retinal reaches a relaxed 13-cis,15-anti configuration. Some of the free energy gain by the retinal will have been lost in lowering the pK_a of the extracellular proton release group to below the pH (i.e., in the unidirectional release).

As long as the Schiff base is unprotonated, the barrier to thermal reisomerization to all-trans is high (41), but a decrease of the pK_a of Asp-96 to near 7 (42) while the pK_a of the Schiff base is 8.5 (43) causes its reprotonation. At this time in the cycle, the remaining excess free energy is no longer stored at the retinal but in the protein: Asp-85 is protonated, Asp-96 is deprotonated, and both extracellular and cytoplasmic regions are rearranged to be consistent with loss and gain of negative charge at these places. When Asp-85 is made permanently neutral (by mutation to Asn), and Asp-96 is made anionic (by lowering its normally high pK_a with a mutation nearby and raising the pH), the retinal isomerizes from all-trans to 13-cis,15-anti in the dark, and as rapidly as in the photocycle (44).

The events that lead back from here to the initial state are driven therefore by the reprotonation of Asp-96 and the deprotonation of Asp-85. The isomeric state of the retinal is coupled (44) to the protonation state of Asp-96, most likely through the aqueous chain of hydrogen bonds that connects them. Indeed, mutations that hinder the reprotonation of Asp-96, or stabilize the aqueous network that locks the Schiff base N-H in the cytoplasmic direction, strongly delay reisomerization to all-trans. In the last photocycle steps, first a distorted all-trans is produced in the O state, and the recovery of the initial geometry is linked to deprotonation of Asp-85 that limits the rate of the last step of the photocycle (45). This last proton transfer is strongly downhill as Asp-85 regains its initial low pK_a , making the recovery of BR the main driving reaction of the photocycle sequence.

Proton Transport or Hydroxyl Ion Transport? The striking sequence similarity between the outward-directed proton pump, bacteriorhodopsin, and the inward-directed chloride ion pump, halorhodopsin, suggests a mechanistic analogy between these proteins. Remarkably, when Asp-85 is replaced with the corresponding residue in halorhodopsin Thr (46) or Ser (47), the proton pump is converted to a chloride ion pump. How the chloride ion is translocated from the extracellular to the cytoplasmic side of the retinal Schiff base is not yet clear but might occur somewhat differently in the two proteins. In D85S bacteriorhodopsin, the bound halide replaces wat402 (19), but in halorhodopsin, the chloride is

at a different location where it is not hydrogen bonded to the Schiff base, the active site Thr, or the homologue of Asp-212 (48). Nevertheless, it seems reasonable to ask whether bacteriorhodopsin might transport hydroxyl ions instead of protons (23, 49, 50).

In one suggested scenario, the Schiff base N-H is rotated to the cytoplasmic direction in L already. Dissociation of wat402 protonates Asp-85, and the hydroxyl ion produced moves to the cytoplasmic side of the Schiff base where it receives its proton (15, 49). This mechanism is at odds with the structure of L and M₁ in Figure 1c,d, where the Schiff base nitrogen continues to point, before and after its deprotonation, to the extracellular direction, and although wat402 has moved somewhat in M₁, it remains on the extracellular side (12, 13). A second scenario is that transfer of the Schiff base proton to Asp-85 is followed by a movement of wat402 across the Schiff base, so the net result is a transfer of a hydroxyl ion in the cytoplasmic direction (50). This mechanism is not contradicted by any reported observation, but as it moves a water molecule instead of an anion across the barrier, it may be considered hydroxyl transport in a conceptual sense only. In a third scenario, consistent with the retinal dynamics in Figure 1, the photocycles of bacteriorhodopsin and halorhodopsin differ only in the way the initially strained 13-cis,15-anti retinal reaches its relaxed configuration in which the Schiff base faces toward the cytoplasmic side. For this to happen in bacteriorhodopsin, a proton must pass from the Schiff base to Asp-85 because rotation of the Schiff base would not be possible without loss of its electrostatic interaction with the immobile anionic Asp-85 (23). In halorhodopsin, however, the counterion, chloride, is mobile, and as the protonated Schiff base nitrogen rotates the hydrogen-bonded chloride ion, it can move with it to the cytoplasmic side (51). Thus, in this alternative, bacteriorhodopsin is able to translocate a proton, and halorhodopsin is able to translocate a chloride ion in the opposite direction, with very similar but not identical mechanisms.

Perspectives. To summarize: proton translocation in bacteriorhodopsin is the result of accommodating the steric and electrostatic mismatch created between the photoisomerized retinal and its binding site. Relaxation of the strains in the chromophore is made possible by conformational changes of the protein that are first local but then spread gradually to the two membrane surfaces. The stages of this cascade, described now in its atomic details and termed local-global conformational coupling, include proton transfers, side-chain rearrangements, and the recruitment of water molecules that facilitate the movement of a proton across the hydrophobic barrier.

Although the driving reaction is different and specific for each ion transporter, the local-global coupling evident in bacteriorhodopsin must be the general principle of all pumps. When the sites for energy input and ion translocation are both inside the membrane bilayer, as for example in cytochrome oxidase, the crucial transport steps occur at the active site, and the global conformational changes need not be large. Such pumps have a close analogy with bacteriorhodopsin (52). Other pumps are more complex. When the two sites are far apart, as for example in the F or V- and P-type ATPases, there is an elaborate machinery to transmit the changes from the extra-membrane driving site to the

intramembrane transport site, by rotational (53) or by pivoting motions (54). Once the intramembrane ion transfers commence in these pumps, however, the questions concerning the affinities of the ion binding sites and the directionality of the ion transfers are much like those in bacteriorhodopsin.

The mechanism of bacteriorhodopsin might be even more relevant to G-protein coupled receptors. Structurally, bacteriorhodopsin is more similar to these heptahelical integral membrane proteins than to the other pumps. The widely differing specificities of the receptors reside in the binding sites, but where best known (55), the global conformational changes that initiate signaling appear to be remarkably similar to those in bacteriorhodopsin. It is possible that the side-chain rearrangements and the ensuing helical tilts that signal to the G-protein are caused by gradual propagation of the local strains introduced at the active site upon binding of the agonist molecule. If that is found to be so, the paradigm of local-global coupling in bacteriorhodopsin will be common principle for transporters and receptors.

REFERENCES

- Haupts, U., Tittor, J., and Oesterhelt, D. (1999) Closing in on bacteriorhodopsin: progress in understanding the molecule, *Annu. Rev. Biophys. Biomol. Struct.* 28, 367–399.
- Lanyi, J. K. (2000) Molecular mechanism of ion transport in bacteriorhodopsin: insights from crystallographic, spectroscopic, kinetic, and mutational studies, *J. Phys. Chem. B* 104, 11441–11448.
- Lanyi, J. K. (2003) Bacteriorhodopsin, *Annual Rev. Physiol.* 66, 11.1–11.24.
- Beja, O. Aravind, L., Koonin, E. V., Suzuki, T., Hadd, A., Nguyen, L. P., Jovanovich, S. B., Gates, C. M., Feldman, R. A., Spudich, J. L., Spudich, E. N., and DeLong, E. F. (2000) Bacterial rhodopsin: evidence for a new type of phototrophy in the sea, *Science* 289, 1902–1906.
- Brown, L. S., Dioumaev, A. K., Needleman, R., and Lanyi, J. K. (1998) Local-access model for proton transfer in bacteriorhodopsin, *Biochemistry* 37, 3982–3993.
- Grigorieff, N., Ceska, T. A., Downing, K. H., Baldwin, J. M., and Henderson, R. (1996) Electron-crystallographic refinement of the structure of bacteriorhodopsin, *J. Mol. Biol.* 259, 393–421.
- Rummel, G., Hardmeyer, A., Widmer, C., Chiu, M. L., Nollert, P., Locher, K. P., Pedruzzi, I., Landau, E. M., and Rosenbusch, J. P. (1998) Lipidic Cubic phases: New matrixes for the three-dimensional crystallization of membrane proteins, *J. Struct. Biol.* 121, 82–91.
- Belrhali, H., Nollert, P., Royant, A., Menzel, C., Rosenbusch, J. P., Landau, E. M., and Pebay-Peyroula, E. (1999) Protein, lipid, and water organization in bacteriorhodopsin crystals: a molecular view of the purple membrane at 1.9 Å resolution, *Struct. Fold. Des.* 7, 909–917.
- Luecke, H., Schobert, B., Richter, H. T., Cartiailler, J. P., and Lanyi, J. K. (1999) Structure of bacteriorhodopsin at 1.55 Å resolution, *J. Mol. Biol.* 291, 899–911.
- Schobert, B., Cupp-Vickery, J., Hornak, V., Smith, S., and Lanyi, J. K. (2002) Crystallographic structure of the K intermediate of bacteriorhodopsin: conservation of free energy after photoisomerization of the retinal, *J. Mol. Biol.* 321, 715–726.
- Matsui, Y., Sakai, K., Murakami, M., Shiro, Y., Adachi, S., Okumura, H., and Kouyama, T. (2002) Specific damage induced by X-ray radiation and structural changes in the primary photo-reaction of bacteriorhodopsin, *J. Mol. Biol.* 324, 469–481.
- Lanyi, J. K., and Schobert, B. (2003) Mechanism of proton transport in bacteriorhodopsin from crystallographic structures of the K, L, M₁, M₂, and M₂' intermediates of the photocycle, *J. Mol. Biol.* 328, 439–450.
- Lanyi, J. K., and Schobert, B. (2002) Crystallographic structure of the retinal and the protein after deprotonation of the Schiff base: the switch in the bacteriorhodopsin photocycle, *J. Mol. Biol.* 321, 727–737.

14. Facciotti, M. T., Rouhani, S., Burkard, F. T., Betancourt, F. M., Downing, K. H., Rose, R. B., McDermott, G., and Glaeser, R. M. (2001) Structure of an early intermediate in the M-state phase of the bacteriorhodopsin photocycle, *Biophys. J.* *81*, 3442–3455.
15. Luecke, H., Schobert, B., Richter, H. T., Cartailler, J.-P., Rosen-garth, A., Needleman, R., and Lanyi, J. K. (2000) Coupling photoisomerization of the retinal in bacteriorhodopsin to directional transport, *J. Mol. Biol.* *300*, 1237–1255.
16. Luecke, H., Schobert, B., Richter, H. T., Cartailler, J. P., and Lanyi, J. K. (1999) Structural changes in bacteriorhodopsin during ion transport at 2 Å resolution, *Science* *286*, 255–261.
17. Subramaniam, S., and Henderson, R. (2000) Molecular mechanism of vectorial proton translocation by bacteriorhodopsin, *Nature* *406*, 653–657.
18. Schobert, B., Brown, L. S., and Lanyi, J. K. (2003) Crystallographic structures of the M and N intermediates of bacteriorhodopsin: assembly of a hydrogen-bonded network of water molecules between Asp96 and retinal Schiff base, *J. Mol. Biol.* *330*, 553–570.
19. Rouhani, S., Cartailler, J.-P., Facciotti, M., Walian, P., Needleman, R., Lanyi, J. K., Glaeser, R. M., and Luecke, H. (2001) Crystal structure of the D85S mutant of bacteriorhodopsin: model of an O-like photocycle intermediate, *J. Mol. Biol.* *313*, 615–628.
20. Neutze, R., Pebay-Peyroula, E., Edman, K., Royant, A., Navarro, J., and Landau, E. M. (2002) Bacteriorhodopsin: a high-resolution structural view of vectorial proton transport, *Biochim. Biophys. Acta* *1565*, 144–167.
21. Smith, S. O., Lugtenburg, J., and Mathies, R. A. (1985) Determination of retinal chromophore structure in bacteriorhodopsin with resonance Raman spectroscopy, *J. Membr. Biol.* *85*, 95–109.
22. Maeda, A., Sasaki, J., Pfeifferlé, J.-M., Shichida, Y., and Yoshizawa, T. (1991) Fourier transform infrared spectral studies on the Schiff base mode of all-*trans* bacteriorhodopsin and its photointermediates, K and L, *Photochem. Photobiol.* *54*, 911–921.
23. Herzfeld, J., and Lansing, J. C. (2002) Magnetic resonance studies of the bacteriorhodopsin pump cycle, *Annu. Rev. Biophys. Biomol. Struct.* *31*, 73–95.
24. Rammelsberg, R., Huhn, G., Lubben, M., and Gerwert, K. (1998) Bacteriorhodopsin's intramolecular proton-release pathway consists of a hydrogen-bonded network, *Biochemistry* *37*, 5001–5009.
25. Spassov, V. Z., Luecke, H., Gerwert, K., and Bashford, D. (2001) pK_a calculations suggest storage of an excess proton in a hydrogen-bonded water network in bacteriorhodopsin, *J. Mol. Biol.* *312*, 203–219.
26. Balashov, S. P., Imasheva, E. S., Govindjee, R., and Ebrey, T. G. (1996) Titration of aspartate-85 in bacteriorhodopsin: what it says about chromophore isomerization and proton release, *Biophys. J.* *70*, 473–481.
27. Richter, H. T., Brown, L. S., Needleman, R., and Lanyi, J. K. (1996) A linkage of the pK_as of Asp-85 and Glu-204 forms part of the reprotonation switch of bacteriorhodopsin, *Biochemistry* *35*, 4054–4062.
28. Brown, L. S., Dioumaev, A. K., Needleman, R., and Lanyi, J. K. (1998) Connectivity of the retinal Schiff base to Asp85 and Asp96 during the bacteriorhodopsin photocycle: the local-access model, *Biophys. J.* *75*, 1455–1465.
29. Dioumaev, A. K., Brown, L. S., Needleman, R., and Lanyi, J. K. (1999) Fourier transform infrared spectra of a late intermediate of the bacteriorhodopsin photocycle suggest transient protonation of Asp-212, *Biochemistry* *38*, 10070–10078.
30. Subramaniam, S., Lindahl, M., Bullough, P., Faruqi, A. R., Tittor, J., Oesterhelt, D., Brown, L., Lanyi, J., and Henderson, R. (1999) Protein conformational changes in the bacteriorhodopsin photocycle, *J. Mol. Biol.* *287*, 145–161.
31. Oka, T., Kamikubo, H., Tokunaga, F., Lanyi, J. K., Needleman, R., and Kataoka, M. (1999) Conformational change of helix G in the bacteriorhodopsin photocycle: investigation with heavy atom labeling and X-ray diffraction, *Biophys. J.* *76*, 1018–1023.
32. Thorgeirsson, T. E., Xiao, W., Brown, L. S., Needleman, R., Lanyi, J. K., and Shin, Y. K. (1997) Transient channel-opening in bacteriorhodopsin: an EPR study, *J. Mol. Biol.* *273*, 951–957.
33. Radzwill, N., Gerwert, K., and Steinhoff, H. J. (2001) Time-resolved detection of transient movement of helices F and G in doubly spin-labeled bacteriorhodopsin, *Biophys. J.* *80*, 2856–2866.
34. Brown, L. S., Needleman, R., and Lanyi, J. K. (2002) Conformational change of the E–F interhelical loop in the M photointermediate of bacteriorhodopsin, *J. Mol. Biol.* *317*, 471–478.
35. Vonck, J. (2000) Structure of the bacteriorhodopsin mutant F219L N intermediate revealed by electron crystallography, *EMBO J.* *19*, 2152–2160.
36. Kataoka, M., Kamikubo, H., Tokunaga, F., Brown, L. S., Yamazaki, Y., Maeda, A., Sheves, M., Needleman, R., and Lanyi, J. K. (1994) Energy coupling in an ion pump. The reprotonation switch of bacteriorhodopsin, *J. Mol. Biol.* *243*, 621–638.
37. Hummer, G., Rasaiah, J. C., and Noworyta, J. P. (2001) Water conduction through the hydrophobic channel of a carbon nanotube, *Nature* *414*, 188–190.
38. Varo, G., Needleman, R., and Lanyi, J. K. (1996) Protein structural change at the cytoplasmic surface as the cause of cooperativity in the bacteriorhodopsin photocycle, *Biophys. J.* *70*, 461–467.
39. Cao, Y., Váró, G., Chang, M., Ni, B., Needleman, R., and Lanyi, J. K. (1991) Water is required for proton transfer from aspartate-96 to the bacteriorhodopsin Schiff base, *Biochemistry* *30*, 10972–10979.
40. Varo, G., and Lanyi, J. K. (1995) Effects of hydrostatic pressure on the kinetics reveal a volume increase during the bacteriorhodopsin photocycle, *Biochemistry* *34*, 12161–12169.
41. Nonella, M., Windemuth, A., and Schulten, K. (1991) Structure of bacteriorhodopsin and in situ isomerization of retinal: a molecular dynamics study, *Photochem. Photobiol.* *54*, 937–948.
42. Zscherp, C., Schlesinger, R., Tittor, J., Oesterhelt, D., and Heberle, J. (1999) In situ determination of transient pK_a changes of internal amino acids of bacteriorhodopsin by using time-resolved attenuated total reflection Fourier transform infrared spectroscopy, *Proc. Natl. Acad. Sci. U.S.A.* *96*, 5498–5503.
43. Brown, L. S., and Lanyi, J. K. (1996) Determination of the transiently lowered pK_a of the retinal Schiff base during the photocycle of bacteriorhodopsin, *Proc. Natl. Acad. Sci. U.S.A.* *93*, 1731–1734.
44. Dioumaev, A. K., Brown, L. S., Needleman, R., and Lanyi, J. K. (1998) Partitioning of free energy gain between the photoisomerized retinal and the protein in bacteriorhodopsin, *Biochemistry* *37*, 9889–9893.
45. Richter, H. T., Needleman, R., Kandori, H., Maeda, A., and Lanyi, J. K. (1996) Relationship of retinal configuration and internal proton transfer at the end of the bacteriorhodopsin photocycle, *Biochemistry* *35*, 15461–15466.
46. Sasaki, J., Brown, L. S., Chon, Y.-S., Kandori, H., Maeda, A., Needleman, R., and Lanyi, J. K. (1995) Conversion of bacteriorhodopsin into a chloride ion pump, *Science* *269*, 73–75.
47. Brown, L. S., Needleman, R., and Lanyi, J. K. (1996) Interaction of proton and chloride transfer pathways in recombinant bacteriorhodopsin with chloride transport activity: implications for the chloride translocation mechanism, *Biochemistry* *35*, 16048–16054.
48. Kolbe, M., Besir, H., Essen, L. O., and Oesterhelt, D. (2000) Structure of the light-driven chloride pump halorhodopsin at 1.8 Å resolution, *Science* *288*, 1390–1396.
49. Luecke, H. (2000) Atomic resolution structures of bacteriorhodopsin photocycle intermediates: the role of discrete water molecules in the function of this light-driven ion pump, *Biochim. Biophys. Acta* *1460*, 133–156.
50. Betancourt, F. M. H., and Glaeser, R. M. (2000) Chemical and physical evidence for multiple functional steps comprising the M state of the bacteriorhodopsin photocycle, *Biochim. Biophys. Acta* *1460*, 106–118.
51. Oesterhelt, D., Hegemann, P., Tavan, P., and Schulten, K. (1986) Trans-cis isomerization of retinal and a mechanism for ion translocation in halorhodopsin, *Eur. Biophys. J.* *14*, 123–129.
52. Wikstrom, M. (1998) Proton translocation by bacteriorhodopsin and heme-copper oxidases, *Curr. Opin. Struct. Biol.* *8*, 480–488.
53. Menz, R. I., Walker, J. E., and Leslie, A. G. (2001) Structure of bovine mitochondrial F(1)-ATPase with nucleotide bound to all three catalytic sites: implications for the mechanism of rotary catalysis, *Cell* *106*, 331–341.
54. Toyoshima, C., Nomura, H., and Sugita, Y. (2003) Crystal structures of Ca²⁺-ATPase in various physiological states, *Ann. N.Y. Acad. Sci.* *986*, 1–8.
55. Hubbell, W. L., Altenbach, C., Hubbell, C. M., and Khorana, H. G. (2003) Rhodopsin structure, dynamics, and activation: a perspective from crystallography, site-directed spin labeling, sulfhydryl reactivity, and disulfide cross-linking, *Adv. Protein Chem.* *63*, 243–290.